

Ultrafast spin-nematic and ferroelectric phase transitions induced by femto-second light pulses

Sangeeta Rajpurohit,^{1,*} Liang Z. Tan,¹ Christian Jooss,² and P. E. Blöchl^{3,4}

¹*Molecular Foundry, Lawrence Berkeley National Laboratory, USA*

²*Institute for Material Physics, Georg-August-Universität Göttingen, Germany*

³*Institute for Theoretical physics, Clausthal University of Technology, Germany*

⁴*Institute for Theoretical Physics, Georg-August-Universität Göttingen, Germany*

Optically-induced phase transitions of the manganite $\text{Pr}_{1/3}\text{Ca}_{2/3}\text{MnO}_3$ have been simulated using a model Hamiltonian, that captures the dynamics of strongly correlated charge, orbital, lattice and spin degrees of freedom. Its parameters have been extracted from first-principles calculations. Beyond a critical intensity of a femto-second light pulse, the material undergoes ultra-fast and non-thermal magnetic phase transition from a non-collinear to collinear antiferromagnetic phases. The light-pulse excites selectively either a spin-nematic or a ferroelectric phase depending on the light-polarization. The behavior can be traced to an optically induced ferromagnetic coupling between Mn-trimers, i.e. polarons which are delocalized over three Mn-sites. The polarization guides the polymerization of the polaronic crystal into distinct patterns of ferromagnetic chains determining the target phase.

The manipulation of local spin order in a magnetic material by electrical or optical means forms the basis of proposed "beyond Moore's Law" information technologies. Photo-induced magnetic phase transitions are possibly the fastest way to alter the spins in magnetic materials, as demonstrated by femtosecond timescale experiments in several ferromagnetic (FM) systems [1–4]. While direct access to the magnetic order in antiferromagnetic and non-collinear spin systems by experiments has been challenging due to very weak or zero net magnetic moments, recent advances have opened new possibilities to use these spin orders as information systems: Optically-induced magnetic phase-transitions have been observed from antiferromagnetic to paramagnetic states in FeBO_3 [5], from collinear to non-collinear antiferromagnetic states in DyFeO_3 [6] and CuO [7]. Inducing weak ferromagnetism through Dzyaloshinskii–Moriya interactions by optically altering local spins in antiferromagnets can be crucial in multiferroicity.

Perovskite manganites are a class of materials with strongly correlated spin, lattice, charge and orbital degrees of freedom.[8–11] This results in a rich phase diagram with long-range ordering patterns. Recently, several fascinating photo-induced phenomena such as magnetic phase transitions, hidden phases, and long-lived excitations have been observed experimentally in the charge- and orbital-ordered manganites [12–15].

In this letter, we report on optically induced, non-thermal magnetic phase transitions in the photo-excited charge- and orbital-ordered stripe-phase $\text{Pr}_{1/3}\text{Ca}_{2/3}\text{MnO}_3$ with non-collinear spin order. The magnetic phase transition is observed above a critical intensity of the light pulse. Two distinct sets of antiferromagnetic patterns can selectively be produced by choosing the polarization direction of the light

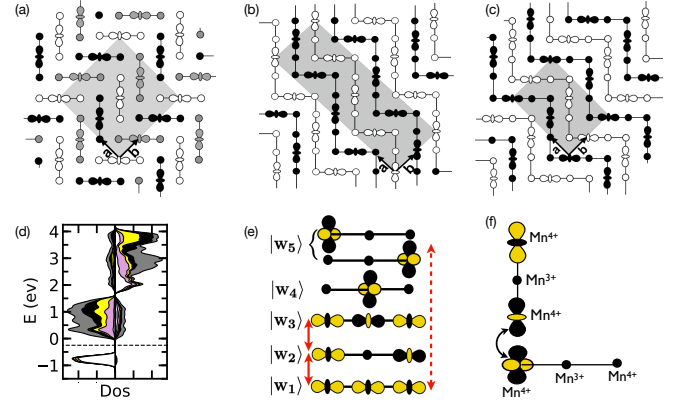


FIG. 1. Charge, orbital, and spin order of $\text{Pr}_{1/3}\text{Ca}_{2/3}\text{MnO}_3$ in (a) the ground state, (b) the spin-nematic phase obtained with a polarization along $\vec{a} + \vec{b}$ and (c) the ferroelectric phase obtained with a polarization along \vec{a} or \vec{b} . The three coplanar spin directions at Mn sites are shown in white, gray, and black. (d) Density of states projected on the Wannier states $|w_1\rangle$ (white), $|w_2\rangle$ (pink), $|w_3\rangle$ (yellow), $|w_4\rangle$ (black) and $|w_5\rangle$ (grey). The right- and left-side shows contribution from majority- and minority-spin states and the dashed line is the Fermi level. (e) Wannier states $|w_i\rangle$ with $i \in \{1, 2, \dots, 5\}$ localized on a Mn-trimer. The red arrows indicate dipole-allowed intra-trimer electronic transitions. (f) $|w_2\rangle$ - $|w_5\rangle$ state hopping of adjacent orthogonal trimers.

pulse: One set of optically induced phases exhibits ferroelectricity. The other set are novel spin-nematic phases with two-fold rotational symmetry. It will be discussed how to selectively drive the system into specific broken-symmetry states and ways to probe them will be suggested. The detailed analysis provides a fairly general picture of optically induced magnetic phase transitions.

The photo-excitation and the subsequent non-equilibrium dynamics presented in the paper is studied

* srajpurohit@lbl.gov

with a tight-binding model for manganites combined with Ehrenfest dynamics. The model captures the strong correlations of electrons, spins and phonons in the manganites. The model, its parameters and the methods used for the Ehrenfest dynamics have been discussed previously [16, 17].

In $\text{Pr}_{1-x}\text{Ca}_x\text{MnO}_3$, the octahedral crystal-field splits the Mn 3d-shell into three non-bonding t_{2g} orbitals and two antibonding e_g states, which are shifted up in energy. In the manganites, the t_{2g} electrons are fully spin polarized and localized. They are described by a spin \vec{S}_R with length $\frac{3}{2}\hbar$ on each Mn-ion. The e_g electrons delocalize via the oxygen bridges connecting the Mn-ions and are described by Pauli-spinor wave functions $|\psi_n\rangle$. The e_g electrons experience an onsite Coulomb interaction, a Hund's coupling to the spins S_R and an electron-phonon coupling with three local phonon modes per Mn-site. The phonon modes are the octahedral breathing $Q_{1,R}$, and the two Jahn-Teller-active modes $Q_{2,R}$ and $Q_{3,R}$. The phonon modes are highly cooperative due to the oxygen ions shared between neighboring MnO_6 octahedra. The spins experience an antiferromagnetic inter-site coupling.

As the perovskite systems are described in the $Pbnm$ space group, we use the corresponding lattice vectors with $\vec{a}||(\vec{e}_y-\vec{e}_x)$, $\vec{b}||(\vec{e}_x+\vec{e}_y)$ and $\vec{c}||\vec{e}_z$, where \hat{e}_x , \hat{e}_y and \hat{e}_z are the directions pointing along the nearest Mn-Mn sites.

The ground state of $\text{Pr}_{1/3}\text{Ca}_{2/3}\text{MnO}_3$ is the so-called stripe phase.[18]. Its charge, orbital and spin order is shown in figure 1.a. Although the charge and orbital order of the stripe-phase $\text{Pr}_{1/3}\text{Ca}_{2/3}\text{MnO}_3$ is well established, its spin order is yet under debate[8, 18, 19]. Based on our calculations, we propose the new spin order, shown in figure 1.a, which has a lower energy than those suggested previously [18–20] [21].

The ground state has a coplanar spin order with three distinct spin axes with an angle of 120° among each other. The spin order in the ab -planes can be understood as an arrangement of trimers. Each trimer is a segment of three ferromagnetically aligned Mn sites in a row along $\vec{a}+\vec{b}$ or $\vec{a}-\vec{b}$ directions in the ab plane. Each trimer is surrounded in the ab -plane by neighboring trimers with a relative spin angle of either $+120^\circ$ or -120° . The ab -planes are antiferromagnetically coupled along the c -axis.

The central Mn-ion of a trimer has a Mn^{3+} oxidation state and the terminal Mn-ions are in the Mn^{4+} oxidation state. Oxidation states are integer by definition. The real charge distribution is more subtle: In our tight-binding model, the formal Mn^{3+} -ions have 0.71 e_g electrons, while the formal Mn^{4+} -ions have 0.145 e_g electrons.

The Jahn-Teller effect lifts the degeneracy of the e_g orbitals at the central Mn^{3+} site and simultaneously distorts its MnO_6 octahedron. The orbital-polarization at Mn^{3+} sites is of $d_{3x^2-r^2}$, respectively $d_{3y^2-r^2}$ -type, [22] and forms a long range orbital-order pattern shown in figure 1.a. The Jahn-Teller distortion at the formal Mn^{4+} ions is smaller, consistent with their e_g occupancy.

Analogously to the half-doped $\text{Pr}_{1-x}\text{Ca}_x\text{MnO}_3$, [16] the electronic structure can be rationalized by Wannier states centered on the trimers. They are shown in Figure 1.e.

The filled states are well represented by the $|w_1\rangle$ Wannier states as seen in the projected density of states 1.d. They have bonding character and a large weight on the Mn^{3+} central sites. Above the Fermi level are the non-bonding $|w_2\rangle$ -states which are localized on the terminal sites of the trimer. The $|w_2\rangle$ states can strongly hybridize with the nearly iso-energetic $|w_5\rangle$ orbitals of a neighboring trimer. The Wannier states with highest energy are the fully antibonding trimer state $|w_3\rangle$ and the upper Jahn-Teller orbital $|w_4\rangle$ of the central site.

To investigate the photo-excitation, we choose a linearly polarized 100-fs light pulse with photon energy $\hbar\omega=0.92$ eV, for which the system exhibits maximum absorption. The electromagnetic field associated with the pulse is $\vec{E}(r,t)=\vec{e}_A\omega\text{Im}(A_oe^{-i\omega t})g(t)$, where A_o is the amplitude of the vector potential, ω is the angular frequency, \vec{e}_A is the direction of the electric field and the Gaussian pulse shape is imposed by $g(t)=e^{-\frac{t^2}{2c_w^2}}(\sqrt{\pi c_w^2})^{-1}$ which has FWHM of $2c_w\sqrt{\ln 2}$. The effect of the electromagnetic field is incorporated in the model through the Peierls substitution as described earlier[17]. A $12\times 12\times 4$ supercell with 576 Mn-ions has been used for the simulations.

To monitor the phase-transition, we use the spin-correlation function

$$C_S(\vec{G})=\frac{1}{N}\left|\sum_{R=1}^N e^{i\vec{G}\vec{R}_R}(\vec{S}_R+\vec{s}_R)\right|^2 \quad (1)$$

where \vec{S}_{R_i} and \vec{s}_{R_i} are the spins of t_{2g} and e_g electrons, respectively, at site R . The wave vector \vec{G} is represented by its relative coordinates (h,k,l) in the $Pbnm$ setting.

The charge and orbital order is monitored by their correlation functions.

The charge-correlation C_Q is $C_Q(\vec{G})=\frac{1}{N}\left|\sum_{R=1}^N e^{i\vec{G}\vec{R}_R}(n_R-\langle n\rangle)\right|^2$, where n_R is the e_g -electron-density at site R and $\langle n\rangle=1/3$ is its average value.

The orbital-correlation function $C_O(\vec{G})$ is $C_O(\vec{G})=\frac{1}{N}\left|\sum_{R=1}^N e^{i\vec{G}\vec{R}_R}(n_{x,R}-n_{y,R})\right|^2$ where $n_{x,R}$ and $n_{y,R}$ are the occupancies of two orthonormal e_g states $|\theta_i\rangle$ with $i\in\{1,2\}$ at site R . [23]

The dynamics of the system has been studied for four different polarization directions of the light-pulse in the ab -plane, namely with the electric field along \vec{a} , \vec{b} , $\vec{a}+\vec{b}$, and $\vec{a}-\vec{b}$.

The excitation leads to two distinct outcomes depending on the polarization of the light pulse:

- A polarization along the oxygen bridges, i.e. parallel to $\vec{a}+\vec{b}$ or $\vec{a}-\vec{b}$, drives the material into a spin-nematic phase shown in figure 1.b.
- A polarization along \vec{a} or \vec{b} leads to a ferroelectric phase shown in figure 1.c.

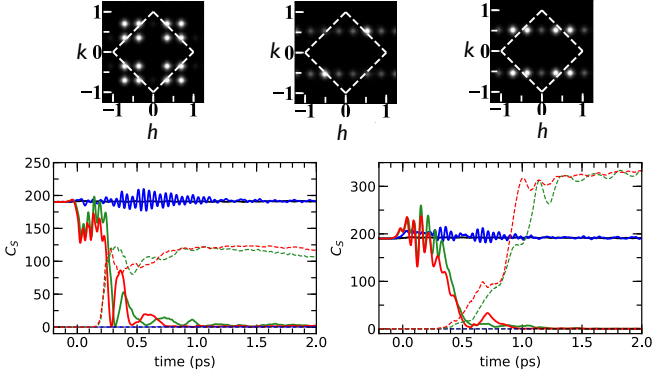


FIG. 2. Top: Spin correlation function C_S for $l=1$ of the ground state (left), the nematic phase obtained by a light pulse polarized along $\vec{a} \pm \vec{b}$ (middle) and the ferroelectric phase obtained with polarization along \vec{a} or \vec{b} . The correlation functions of the optically induced phases are shown for 1 ps after the pulse. Bottom: Time evolution of the spin correlation function at $(1/2, 1/2, 1)$ characteristic for the spin-nematic phase (left) and at $(1/3, 1/2, 1)$, which is characteristic for the ferroelectric phase (right). The full lines show the spin correlation at $(1/3, 1/3, 1)$ characteristic for the ground state. The colors refer to the increasing intensities with $A_0 = 0.10 \hbar/ea_o$ (black), $0.225 \hbar/ea_o$ (blue), $0.45 \hbar/ea_o$ (green) and $0.50 \hbar/ea_o$ (red). The corresponding photon absorptions per Mn D_p for polarization along \vec{b} ($\vec{a} + \vec{b}$) are $D_p = 0.002(0.001)$ ph/Mn (black), $0.016(0.015)$ ph/Mn (blue), $0.047(0.039)$ ph/Mn (green) and $0.062(0.043)$ ph/Mn (red).

The spin-correlation functions for the ground state and the two optically-induced phases are shown in figure 2. The order parameter for the transition is the spin-correlation function at specific reciprocal lattice vectors. Their time dependence demonstrating the ultra-fast response on a sub-picosecond time scale is shown in figure 2.

- The coplanar spin order of the ground state displays strong peaks in the spin-correlation C_S at wave vectors $(h, k, l) = (u \pm 1/3, v \pm 1/3, 2w - 1)$ with integer u, v, w and independent \pm .
- The spin-nematic phases are characterized by two sets of C_S peaks. The first set appears at wave vectors $(h, k, l) = (u + 1/2, v + 1/2, 2w - 1)$ with integer u, v, w with even $u + v$. The second set, 4-5 times weaker, has wave vectors $(h, k, l) = (u \pm 1/6, v - 1/2, 2w - 1)$ with integer u, v, w .
- The ferroelectric phases have strong C_S peaks at wave vectors $(h, k, l) = (u \pm 1/3, v + 1/2, 2w - 1)$ with integer u, v, w .

Let us first describe the excitation by light polarized parallel to the oxygen bridges, that is along $\vec{a} + \vec{b}$ or $\vec{a} - \vec{b}$. These polarizations results in the spin-nematic phases. The excitation takes place at those trimers that are aligned with the electric field. The excitation lift electrons from the Wannier state $|w_1\rangle$, shown in figure 1.e, to

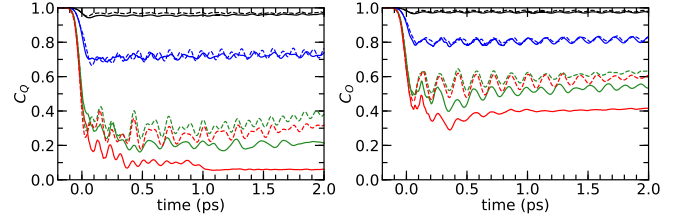


FIG. 3. Charge correlation C_Q at $(h, k, l) = (1/3, 1, 0)$ and orbital correlation C_O at $(h, k, l) = (1/3, 0, 0)$ as function of time for light pulses polarized along \vec{b} (dashed lines) and $(\vec{a} + \vec{b})$ (solid lines). The intensities are color coded as described in figure 2

the antisymmetric state $|w_2\rangle$. The corresponding dipole oscillation shuffles charge between the two terminal Mn-sites of the excited trimer.

Furthermore, by shifting weight from $|w_1\rangle$ to $|w_2\rangle$, the excitation transfers charge from the central atom to the terminal atoms of the trimer. This charge transfer can be observed by the sudden drop in the charge correlation in figure 3.

Via electron-phonon coupling, the charge transfer excites phonons, which are in turn responsible for the oscillations of the charge and orbital correlation functions in figure 3. These phonons are closely related to the long-lived coherent phonons in $\text{Pr}_{1/2}\text{Ca}_{1/2}\text{MnO}_3$ [17], which have been observed experimentally in $\text{Pr}_{1/2}\text{Ca}_{1/2}\text{MnO}_3$ [13, 24] In contrast to the half-doped material,[16] these phonons are damped out more rapidly after the optically induced phase transition, both for the spin-nematic phase and for the ferroelectric transition.

The excited Wannier state $|w_2\rangle$ has a large spatial overlap with a $|w_5\rangle$ Wannier state of an adjacent orthogonal trimer as shown schematically in figure 1.f. This causes a charge transfer between the two adjacent trimers, or, in other words, the formation of an inter-trimer bond. The two Wannier states, $|w_2\rangle$ and $|w_5\rangle$, have, however, a spin angle of 120° . Because the electron transfer between $|w_2\rangle$ and $|w_5\rangle$ Wannier states is limited to the like-spin component, the spin of the e_g electrons in the $|w_5\rangle$ Wannier state aligns with the excited trimer. Hund's rule coupling, in turn, leads to a force on the t_{2g} spins S_R , which aligns them with the new spin direction of the e_g electrons. This introduces an effective ferromagnetic coupling between adjacent, orthogonal trimers within chains having five Mn sites in a segment along the polarization direction and three sites in the orthogonal direction. Beyond a critical intensity of the light pulse, provided in table I, the effect is sufficiently strong to drive the system through the phase transition towards the spin-nematic phase of figure 1.

The co-planar spins of trimers in a chain with spin-angles of 120° align ferromagnetically by adding an out-of-plane spin component, while reducing the in-plane

TABLE I. Critical intensities for the optically induced magnetic, charge- and orbital-order phase transitions. A_0 is the amplitude of the vector potential and D_p is photon absorption in number of absorbed photons per Mn site.

polarization unit phase transition	$\vec{a} + \vec{b}, \vec{a} - \vec{b}$		\vec{a}, \vec{b}	
	$\hbar/(ea_0)$ A_0	ph/Mn D_p	$\hbar/(ea_0)$ A_0	ph/Mn D_p
magnetic	0.25	0.019	0.40	0.032
charge order	1.00	0.088	0.65	0.097
orbital order	1.60	0.168	1.20	0.158

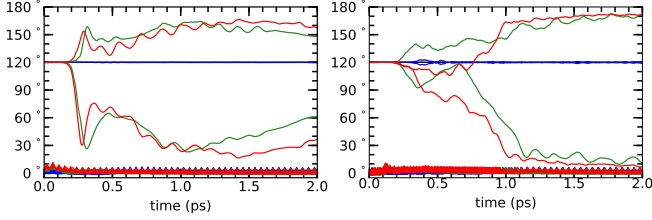


FIG. 4. Spin angles of adjacent Mn-trimers as function of time for light polarized along $\vec{a} + \vec{b}$ (left) and along \vec{b} (right). The trimers are grouped according to their final spin alignment parallel or antiparallel to the global spin axis. On average, the spins deviate by less than 15° from the spin axis of the trimer they reside on (triangles). Individual spins may deviate up to 30° . The colors (black, blue, green, red) indicate increasing intensities of the light pulse as quantified in figure 2.

components as seen from figure 4. The spins reach a ferromagnetic alignment for the first time at approximately 0.3 ps after the light pulse. This event is followed by a longer sequence of spin fluctuations on the picosecond time scale. The conservation of the total spin results in a complex spin transfer between different chains during this period.

Depending on the polarization, the ferromagnetic chains assume one of two spatial directions, which differ by an angle of 37° . A polarization along $\vec{a} + \vec{b}$ leads to a chain with an angle of 18° with the \vec{a} -axis and 72° with the \vec{b} -axis. A polarization along $\vec{a} - \vec{b}$ leads to a phase which is obtained from the first by an inversion at the Mn^{3+} ion. Interestingly the Mn^{3+} remain at their positions as long as the charge order does not melt.

After having described the dynamics for a polarization along the Mn-trimers, let us now turn to the polarization along \vec{a} or \vec{b} . A light pulse polarized with a 45° angle from the trimer axes, results in a quite different behavior. In this case a ferromagnetic coupling between adjacent orthogonal trimer is established as in the case described above. However, each terminal site of a trimer can connect to one of two different orthogonal trimers. One might thus anticipate a pattern with chains made of a random sequence of straight sections with 3, 4 and 5 Mn-sites. However, the simulations only show

patterns with segments having 4 Mn-sites. This can be attributed to the fact that each such chain already has a dominant spin axis in the ground state, figure 1.a, because the spin angles of the trimers within such a chain alternate between only two rather than three spin orientations with an angle of 120° . The preference of a spin-orientation, build already in the ground state selects a particular pattern, namely four-membered segments, after the magnetic phase transition.

There are two possible ferroelectric orientations, along $+\vec{a}$ and $-\vec{a}$, which form without apparent preference. Both patterns break inversion symmetry and are ferroelectric with a polarization vector parallel to the a -axis. The ferroelectric dipole is formed by the inner two Mn-sites, a formal Mn^{3+} and a formal Mn^{4+} ion, of a four-site segment.

As seen in figure 2 and 4, the spin dynamics leading to the ferroelectric phases is considerably slower than that leading to the spin-nematic phase. The order parameter for the ferroelectric transition settles after 1 ps as compared to 0.3 ps for the spin-nematic phase. This may be due to the competition between ferroelectric domains, which have distinct patterns of ferromagnetic chains. Furthermore, the preferred spin axes of the ferromagnetic chains in the ferroelectric transition form themselves a spin spiral along the \vec{b} -axis. The transition from this spin spiral to a collinear antiferromagnetic order is frustrated.

The charge and orbital orders are more stable and melt at considerably higher intensities than the optically-induced magnetic transitions as shown in table I.

In conclusion, our simulations demonstrate the possibility of ultrafast manipulation of the magnetic order by ultra-short (femto-second) light pulses. The materials studied exhibit a strongly intertwined charge-, orbital- and non-collinear spin order. The polarization direction allows to drive the system selectively into a spin-nematic phase or a ferroelectric phase. The particular broken-symmetry state of the spin-nematic phase can be produced selectively by the choice of the polarization. The selection of a particular broken-symmetry state of the ferroelectric phase requires an additional electric field. This field may be static or due to a simultaneous terahertz light pulse with a phase synchronized with the light pulse.

The optically-induced magnetic phase transitions discussed here can be investigated experimentally through ultrafast pump-probe experiments with linearly polarized pulses. The spin dynamics is accessible via time-resolved neutron diffraction [8, 18] or magneto-optical Kerr spectroscopy [25, 26].

Photo-induced magnetic phase transitions open possibilities for ultrafast manipulation and storage of information exploiting polarization-sensitive coupling between solid-state and photonic systems.

The present research work was supported by the Computational Materials Sciences Program funded by the US Department of Energy, Office of Science, Basic En-

ergy Sciences, Materials Sciences and Engineering Division. Financial support from the Deutsche Forschungsge-

meinschaft (DFG, German Research Foundation) (Grant No 217133147/SFB1073) through Projects B02, B03 and C03 is gratefully acknowledged.

-
- [1] E. Beaupaire, J.-C. Merle, A. Daunois, and J.-Y. Bigot, *Phys. Rev. Lett.* **76**, 4250 (1996).
- [2] J. Hohlfeld, E. Matthias, R. Knorren, and K. H. Bennemann, *Phys. Rev. Lett.* **78**, 4861 (1997).
- [3] J. Gdde, U. Conrad, V. Jhnke, J. Hohlfeld, and E. Matthias, *Phys. Rev. B* **59**, R6608 (1999).
- [4] A. Kirilyuk, A. V. Kimel, and T. Rasing, *Rev. Mod. Phys.* **82**, 2731 (2010).
- [5] A. V. Kimel, R. V. Pisarev, J. Hohlfeld, and T. Rasing, *Phys. Rev. Lett.* **89**, 287401 (2002).
- [6] D. Afanasiev, B. A. Ivanov, A. Kirilyuk, T. Rasing, R. V. Pisarev, and A. V. Kimel, *Phys. Rev. Lett.* **116**, 097401 (2016).
- [7] S. L. Johnson, R. A. de Souza, U. Staub, P. Beaud, E. Mhr-Vorobeva, G. Ingold, A. Caviezel, V. Scagnoli, W. F. Schlotter, J. J. Turner, O. Krupin, W.-S. Lee, Y.-D. Chuang, L. Patthey, R. G. Moore, D. Lu, M. Yi, P. S. Kirchmann, M. Trigo, P. Denes, D. Doering, Z. Hussain, Z.-X. Shen, D. Prabhakaran, and A. T. Boothroyd, *Phys. Rev. Lett.* **108**, 037203 (2012).
- [8] Z. Jirk, S. Krupicka, Z. Simsa, M. Dlouh, and S. Vratislav, *Journal of Magnetism and Magnetic Materials* **53**, 153 (1985).
- [9] P. Schiffer, A. P. Ramirez, W. Bao, and S.-W. Cheong, *Phys. Rev. Lett.* **75**, 3336 (1995).
- [10] Y. Tokura, *Reports on Progress in Physics* **69**, 797 (2006).
- [11] C. Jooss, L. Wu, T. Beetz, R. F. Klie, M. Belligia, M. A. Schofield, S. Schramm, J. Hoffmann, and Y. Zhu, *Proceedings of the National Academy of Sciences* **104**, 13597 (2007), <http://www.pnas.org/content/104/34/13597.full.pdf>.
- [12] T. Li, A. Patz, L. Mouchliadis, J. Yan, T. A. Lograsso, I. E. Perakis, and J. Wang, *Nature* **496**, 69 EP (2013).
- [13] P. Beaud, A. Caviezel, S. O. Mariager, L. Rettig, G. Ingold, C. Dornes, S.-W. Huang, J. A. Johnson, M. Radovic, T. Huber, T. Kubacka, A. Ferrer, H. T. Lemke, M. Chollet, D. Zhu, J. M. Glownia, M. Sikorski, A. Robert, H. Wadati, M. Nakamura, M. Kawasaki, Y. Tokura, S. L. Johnson, and U. Staub, *Nature Materials* **13**, 923 (2014).
- [14] D. Raiser, S. Mildner, B. Iffland, M. Sotoudeh, P. Blchl, S. Techert, and C. Jooss, *Advanced Energy Materials* **7**, 1602174 (2017), 1602174.
- [15] H. Lin, H. Liu, L. Lin, S. Dong, H. Chen, Y. Bai, T. Miao, Y. Yu, W. Yu, J. Tang, Y. Zhu, Y. Kou, J. Niu, Z. Cheng, J. Xiao, W. Wang, E. Dagotto, L. Yin, and J. Shen, *Phys. Rev. Lett.* **120**, 267202 (2018).
- [16] M. Sotoudeh, S. Rajpurohit, P. Blchl, D. Mierwaldt, J. Norpoth, V. Roddatis, S. Mildner, B. Kressdorf, B. Iffland, and C. Jooss, *Phys. Rev. B* **95**, 235150 (2017).
- [17] S. Rajpurohit, C. Jooss, and P. E. Blchl, *Phys. Rev. B* **102**, 014302 (2020).
- [18] P. G. Radaelli, D. E. Cox, L. Capogna, S.-W. Cheong, and M. Marezio, *Phys. Rev. B* **59**, 14440 (1999).
- [19] Z. Jirk, C. Martin, M. Hervieu, and J. Hejtmnek, *Applied Physics A* **74**, s1755 (2002).
- [20] T. Hotta, Y. Takada, H. Koizumi, and E. Dagotto, *Phys. Rev. Lett.* **84**, 2477 (2000).
- [21] The previously proposed collinear [20] and non-collinear[8, 18, 19] spin orders have been used as initial states for the optimization.
- [22] The occupied e_g orbitals at Mn^{3+} sites are linear combination of e_g states $|\theta\rangle = -|x^2 - y^2\rangle \sin(\theta) + |3z^2 - r^2\rangle \cos(\theta)$ with $\theta=60^\circ$ which suggests almost $d_{3x^2-r^2}/d_{3y^2-r^2}$ -type orbital-polarization.
- [23] The states $|\theta_i\rangle = |x^2 - y^2\rangle \sin(\theta_i/2) + |3z^2 - r^2\rangle \cos(\theta_i/2)$ with $\theta_x = \pi$ and $\theta_y = 2\pi/3$, i.e. with nearly axial lobes along x and y , are chosen consistent with resonating x-ray diffraction experiments at Mn-K edge [27], which involve 1s-to-4p states Mn transitions.
- [24] V. Esposito, L. Rettig, E. Abreu, E. M. Bothschafter, G. Ingold, M. Kawasaki, M. Kubli, G. Lantz, M. Nakamura, J. Rittman, M. Savoini, Y. Tokura, U. Staub, S. L. Johnson, and P. Beaud, *Phys. Rev. B* **97**, 014312 (2018).
- [25] W. Feng, G.-Y. Guo, J. Zhou, Y. Yao, and Q. Niu, *Phys. Rev. B* **92**, 144426 (2015).
- [26] M. Wu, H. Isshiki, T. Chen, T. Higo, S. Nakatsuji, and Y. Otani, *Applied Physics Letters* **116**, 132408 (2020), <https://doi.org/10.1063/1.5143959>.
- [27] M. v. Zimmermann, C. S. Nelson, J. P. Hill, D. Gibbs, M. Blume, D. Casa, B. Keimer, Y. Murakami, C.-C. Kao, C. Venkataraman, T. Gog, Y. Tomioka, and Y. Tokura, *Phys. Rev. B* **64**, 195133 (2001).